Chinese Chemical Letters 31 (2020) 2742–2746

Contents lists available at ScienceDirect

Chinese Chemical Letters

journal homepage: www.elsevier.com/locate/cclet

Communication

Adsorption performance and mechanism of Schiff base functionalized polyamidoamine dendrimer/silica for aqueous Mn(II) and Co(II)

Wenzhu Qiao, Peixu Zhang, Lixiang Sun, Songmei Ma, Wenlong Xu, Shengguang Xu, Yuzhong Niu*

School of Chemistry and Materials Science, Ludong University, Yantai 264025, China

ARTICLE INFO

Article history:
Received 29 February 2020
Received in revised form 2 April 2020
Accepted 22 April 2020
Available online 30 April 2020

Keywords:
Adsorption
Schiff base
PAMAM dendrimer
DFT calculation

ABSTRACT

Schiff base functionalized polyamidoamine (PAMAM) dendrimer/silica were prepared for the adsorption of aqueous Mn(II) and Co(II). The effects that influence the adsorption were investigated systematically and the adsorption mechanism was illustrated by theoretical calculation. The optimum adsorption pH are 4 and 6 for Mn(II) and Co(II). Adsorption kinetics follow pseudo-second-order model and the rate-controlling step is film diffusion process. Adsorption isotherm shows that high initial metal ion concentration facilitates the uptake of metal ions. The adsorption capacity increases first and then decreases in the temperature range of 15–35 °C. Density functional theory (DFT) calculation demonstrates that Schiff base functionalized PAMAM dendrimer tends to coordinate Mn(II) and Co(II) with the oxygen atoms of hydroxyl and carbonyl groups, nitrogen of tertiary amine and imino groups. The imino and tertiary amine groups mainly dominate the adsorption. The reproducibility of the adsorbents indicates they can be regenerated by 5% thiourea and 0.5 mol/L HNO_3 solution efficiently.

Water pollution caused by heavy metal ions has become a serious problem. These toxic ions pose severe threat to ecological system and human health due to the non-biodegradable characteristic [1]. Among these ions, Mn(II) and Co(II) are usually discharged from battery, alloy, and metallurgical industries [2,3]. And they are usually presented together in the wastewater of lithium battery industry for the production cathode material. The uptake of Mn(II) may cause hallucinations, psychiatric abnormalities and violent acts [4]. And the ingestion of Co(II) can cause paralysis, lung irritation, and diarrhea [3]. Hence, the elimination of aqueous Mn(II) and Co(II) is of great significance for the remediation of environmental pollution.

Various methods have been used to decontaminate heavy metal ions, such as ion exchange, membrane separation, adsorption, and chemical precipitation [5]. Adsorption is considered as an effective and economical technique because of its low cost, simplicity, high efficiency, and regeneration of the adsorbents [6]. In the past few years, adsorbents such as chitosan [7], silica [4], magnetic composite [8], metal-organic framework materials [9], and activate carbon [10] were employed to adsorb Mn(II) and Co(II). Therefore, the design of effective adsorbents is still of urgent.

PAMAM dendrimers represent a class of fascinating functional groups [11]. The presence of abundant oxygen and nitrogen endows them remarkable binding affinity to heavy metal ions [12]. However, both PAMAM dendrimer and its metal ion complex are generally soluble in aqueous solution, which makes it hard for the separation after adsorption. Therefore, PAMAM dendrimers are usually immobilized on the support materials such as magnetic nanoparticles, silica, chitosan, polystyrene, and graphene oxide [11]. Among these support materials, silica has been widely used due to the advantages of the large surface area, outstanding thermal and chemical stability, easy functionalization, and high porosity [13,14]. The incorporation of silica would facilitate the separation by filtration after adsorption and the regeneration of the adsorbent. For example, Wu *et al.* prepared PAMAM dendrimer functionalized silica to separate Pd(II) from aqueous solution [15]. Gao *et al.* synthesized EDTA-terminated PAMAM dendrimer/silica composites for the selective adsorption of Zn(II), Pb(II) and Cr(III) [16]. Our group also synthesized a series of ester- and amino-terminated PAMAM dendrimer modified silica for the adsorption of Pb(II) and Hg(II) [17]. Results indicate the terminal groups of PAMAM dendrimer greatly affect the adsorption performance. Schiff base functional group which is formed *via* the reaction of amino and carbonyl groups has been demonstrated to exhibit marked binding affinity for metal ions [5]. Hence, it can be reasonable concluded that the incorporation of Schiff base

* Corresponding author.
E-mail address: niuyuzhong@ldu.edu.cn (Y. Niu).

https://doi.org/10.1016/j.cclet.2020.04.036

functional group to the periphery of PAMAM dendrimer would improve the adsorption property of the adsorbent. Hence, Schiff base functionalized PAMAM dendrimer/silica (SiO_2-G0-SA, SiO_2-G1.0-SA, and SiO_2-G2.0-SA, Scheme S1 in Supporting information) were synthesized for the removal of aqueous Mn(II) and Co(II). The adsorption performance and mechanism was illustrated based on experimental and theoretical results. The reproducibility of the adsorbents was also determined.

First, γ-aminopropyltriethoxysilane was used for the surface modification of silica (100–200 mesh) to introduce amino groups (SiO_2-G0). Then, the first and second generations PAMAM dendrimer were grafted onto silica (SiO_2-G1.0 and SiO_2-G2.0) by the interactive Mikael addition of methyl acrylate with amino group and the subsequent amidation of ester group with ethylenediamine. Finally, SiO_2-G0-SA, SiO_2-G1.0-SA, and SiO_2-G2.0-SA were achieved by the decoration of SiO_2-G0, SiO_2-G1.0 and SiO_2-G2.0 by salicylaldehyde [18]. The detail synthesis procedures are provided in Text S1 (Supporting information).

The adsorption performance of the as-synthesized adsorbents for Mn(II) and Co(II) was evaluated by considering the adsorption capacity, effect of solution pH, adsorption isotherm and kinetic. The detailed adsorption procedures and analytical methods were introduced in Text S2 (Supporting information). The adsorption capacity for Mn(II) and Co(II) are presented in Fig. 1. The adsorption capacity for Mn(II) follows the trend of SiO_2-G0-SA < SiO_2-G1.0-SA < SiO_2-G2.0-SA, suggesting the adsorption capacity for Mn(II) increases with the increase of dendrimer generation. The favorable adsorption of Mn(II) by high generation Schiff base functionalized PAMAM dendrimer is owed to the high content of nitrogen and oxygen functional group [18]. Unlike Mn(II), the adsorption amount for Co(II) increases first and then decreases by following the trend of SiO_2-G0-SA < SiO_2-G2.0-SA < SiO_2-G1.0-SA. The possible reason for this phenomenon is due to the higher binding ability of peripheral Schiff base functional groups for Co(II) as compared with Mn(II). During the initial adsorption process, Co(II) is preferred to be captured by the surface functional group first and surface network would be formed due to the coordination. As the content of surface functional group of SiO_2-G2.0-SA is higher than SiO_2-G1.0-SA, the steric hindrance of SiO_2-G2.0-SA that caused by the network structure is also higher than SiO_2-G1.0-SA, which blocks the diffusing the Co(II) into the interior structure of the dendrimer, resulting in the decrease of the adsorption capacity for SiO_2-G2.0-SA. Similar results was also observed for Co(II) and Pb(II) adsorption by PAMAM dendrimer functionalized silica in previous reports [17,19].

The effect of solution pH on the adsorption of Mn(II) and Co(II) are presented in Fig. S1 (Supporting information). The adsorption capacity for Mn(II) increases with the solution pH raise from 1 to 4, and then decreases in the pH range of 4−6. The functional groups of Schiff base functionalized PAMAM dendrimer such as −OH and –NH– are protonated into the form of $-OH_2^+$ and $-NH_2^+-$ at low pH, leading to the loss of binding ability for Mn(II) [4]. Furthermore, the strong electrical repulsion between the positively charged surface and Mn(II) also prevents Mn(II) from contacting with the adsorbent. The functional groups are deprotonated gradually with the pH increases, leading to the recovery of binding ability of the adsorbent. Thus, the adsorption capacity increases accordingly with the solution pH increases. When the pH continue increasing, Mn(II) will be hydrolyzed and presented in the forms of $MnOH^+$ and $Mn(OH)_2$, which would cause invalid adsorption for Mn(II) [21]. Similar phenomena were also reported for the adsorption of Mn(II) by Na-Clinoptilolite [22] and *Spirodela polyrhiza* (L.) Schleiden biomass adsorbent [23]. For Co(II), the adsorption capacity increases in the pH range of 1–6 and achieves the optimum adsorption at pH 6. The low adsorption capacity for Co(II) at low solution pH is similar to that of Mn(II).

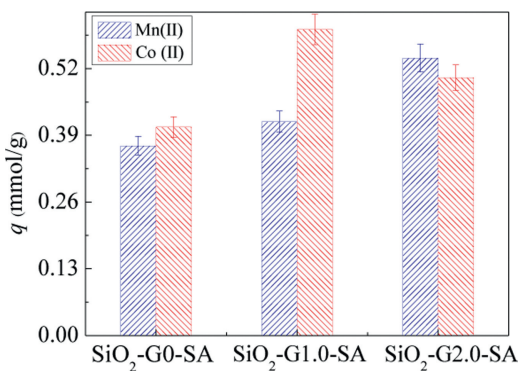

Fig. 1. The adsorption capacity for Mn(II) and Co(II) (T = 25 ℃, C = 0.005 mol/L).

The adsorption kinetic plots for Mn(II) and Co(II) are illustrated in Fig. 2. The adsorption is very rapid in the first 80 and 50 min for Mn(II) and Co(II), respectively. Then, it gradually retards until approaches equilibrium at 105 min for both Mn(II) and Co(II). The rapid uptake of metal ion at the initial stage is mainly ascribed to the existence of plenty binding sites of the adsorbent and high metal ion concentration, which facilitates the capture of metal ion by the adsorbent. With the proceeding of the adsorption, both the metal ion concentration and binding sites decrease, resulting in the slowdown of the adsorption. Moreover, the adsorbed Mn(II) and Co(II) could form chelate with the surface functional group of Schiff base functionalized PAMAM dendrimer, which also hinders the diffusion of metal ion into the interior of the adsorbents and decrease the adsorption rate [19].

Pseudo-first-order and *pseudo*-second-order kinetic models in Text S2 were adopted to reveal the adsorption kinetic mechanism [24]. The fitting plots of *pseudo*-second-order kinetic models and the corresponding parameters of the two models are collected in Fig. S2 and Table S1 (Supporting information). According to Fig. S2 and Table S1, the adsorption kinetic for both Mn(II) and Co(II) can be depicted by *pseudo*-second-order kinetic model due to the relative high correlation coefficients (R_2^2). Furthermore, the calculated adsorption capacity ($q_{e,cal}$) from *pseudo*-second-order model is close to the experimental data ($q_{e,exp}$), further demonstrating it is more suitable to describe the adsorption kinetic process of Mn(II) and Co(II) by *pseudo*-second-order model. Similar results were also indicated for the removal of Mn(II) and Co(II) by Fe_3O_4 nanoparticles [25], Mg-Zn-Al LDH/montmorillonite [26], and rice husk [27].

Boyed film diffusion model in Text S2 was employed to determine whether the rate-controlling step is film diffusion or intraparticle diffusion [28]. The fitting result is presented in Table S2 (Supporting information), the result indicates the adsorption of Mn(II) and Co(II) is dominated by film diffusion process as the fitting plots of *Bt versus t* display excellent linearity without passing through the origin [29].

Adsorption isotherm can be used to depict the interactive behavior between adsorbent and adsorbate. The adsorption isotherm curves for Mn(II) and Co(II) are showed in Fig. 3. With the increase of initial metal ion concentration, the adsorption increases accordingly due to the presence of higher driving force under high concentration. The diffusion of metal ion would be promoted by the higher driving force and the adsorption would be enhanced. It can be also found temperature has a remarkable effect on the adsorption capacity. The adsorption capacity for Mn(II) and Co(II) increase first in the range of 15–25 °C, and then decrease when the temperature rises to 35 °C. In the temperature ranges of 15–25 °C, the molecular motion degree of PAMAM dendrimer and metal ion increases, which facilitate the capture of metal ion by the adsorbents. With the temperature gradually rises to 35 °C, the

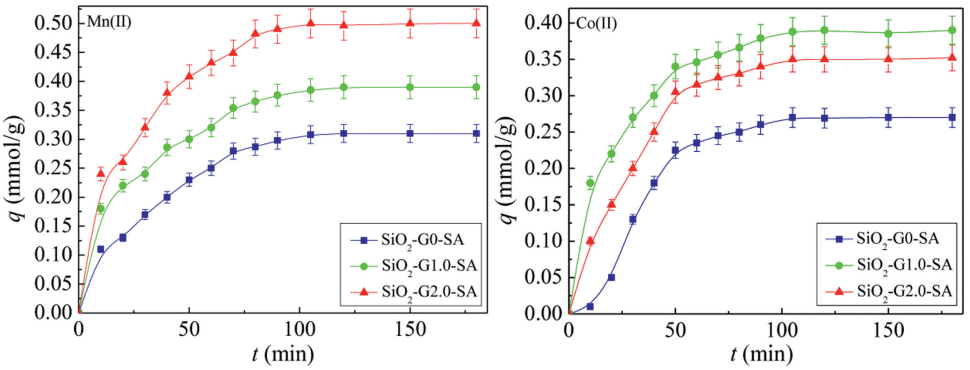

Fig. 2. Adsorption kinetic curves of Mn(II) and Co(II) (T = 25 °C, $C_{Mn(II)}$ = 0.003 mol/L, pH 4, $C_{Co(II)}$ = 0.002 mol/L, pH 6).

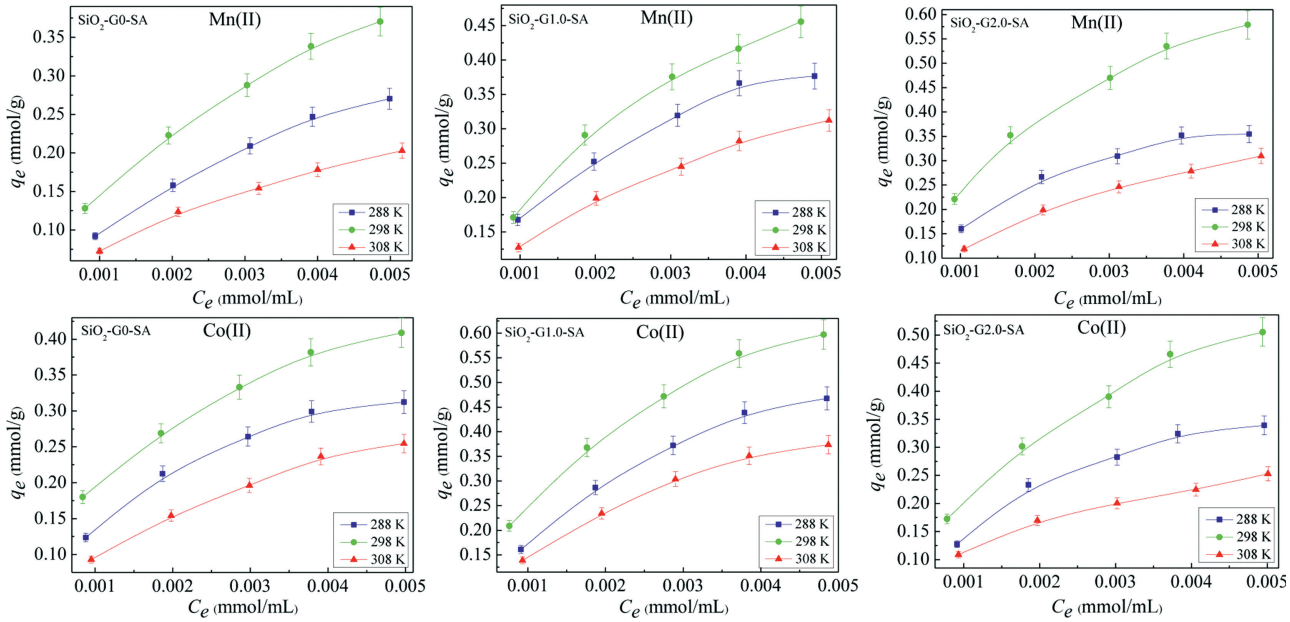

Fig. 3. The adsorption isotherms for Mn(II) and Co(II) (C = 0.001–0.006 mol/L, $pH_{Mn(II)}$ 4, $pH_{Co(II)}$ 6).

degree of molecular motion continue increasing. Therefore, the force of molecular movement may exceed the binding affinity of the adsorbent for metal ion, resulting in the escape of metal ion from the chelating of the adsorbent [16]. Hence, the adsorption capacity decrease with the temperature increase from 25 °C to 35 °C. Similar phenomena were also observed for the uptake of Co(II), Hg(II), and Cr(VI) by silica supported PAMAM dendrimer, mercapto-functionalized silica, and chitosan, *etc.* [19,30,31].

Langmuir, Freundlich, and Dubinin–Radushkevich (D-R) models in Text S2 were adopted to evaluate the adsorption isotherm mechanism [4,32]. The fitting plots of Langmuir model are illustrated in Fig. S3 (Supporting information) and the calculated parameters of Freundlich and Langmuir models are reported in Table S3 (Supporting information), Langmuir model provides more accurate description for Mn(II) and Co(II) adsorption than Freundlich model due to the higher correlation coefficients (R_L^2). The maximum adsorption capacity (q_m) obtained from Langmuir model is closer to the experiment data, further suggesting Langmuir model is appropriate to describe the adsorption process. These results demonstrate the uptake of Mn(II) and Co(II) is proceeded by monolayer adsorption behavior. The comparison of the q_m of the as-prepared adsorbents for Mn(II) and Co(II) with other reported adsorbents is provided in Table S4 (Supporting information). It shows that the as-prepared adsorbents show relative high adsorption capacity than most of the reported adsorbents, indicating the adsorbents have competitive adsorption performance. Especially, the as-prepared adsorbents exhibit higher adsorption capacity toward Mn(II) and Co(II) than the corresponding PAMAM dendrimer/silica adsorbent [19,33]. Take SiO_2-G2.0-SA for example, the q_m for Mn(II) is 0.92 mmol/g, which is higher than the corresponding PAMAM dendrimer/silica (SiO_2-G2.0-SA) by 0.32 mmol/g. The result indicates the adsorption capacity of SiO_2-G2.0-SA was enhanced by 53.33% after modification with Schiff base functional group. Thus, they can be used potentially for the removal of aqueous Mn(II) and Co(II) as efficient adsorbents.

D-R model is used to confirm whether the adsorption is physical or chemical. The mean free energy (E, kJ/mol) obtained from D-R model can be employed as the criterion to judge the nature of the adsorption. If the value of E lies in the range of 8–16 kJ/mol, the adsorption is belonged to chemical adsorption. When the E value is lower than 8 kJ/mol, the adsorption is mainly dominated by physical adsorption [5]. The fitting results of D-R model are listed in Table S5 (Supporting information). Except the adsorption of SiO_2-G0-SA for Mn(II), SiO_2-G1.0-SA and SiO_2-G2.0-SA for Co(II) at 15 °C, the E values for Mn(II) and Co(II) by the adsorbents are all in the range of 8–16 kJ/mol, suggesting the adsorption of Mn(II) and Co(II) are mainly attributed to the chemical adsorption.

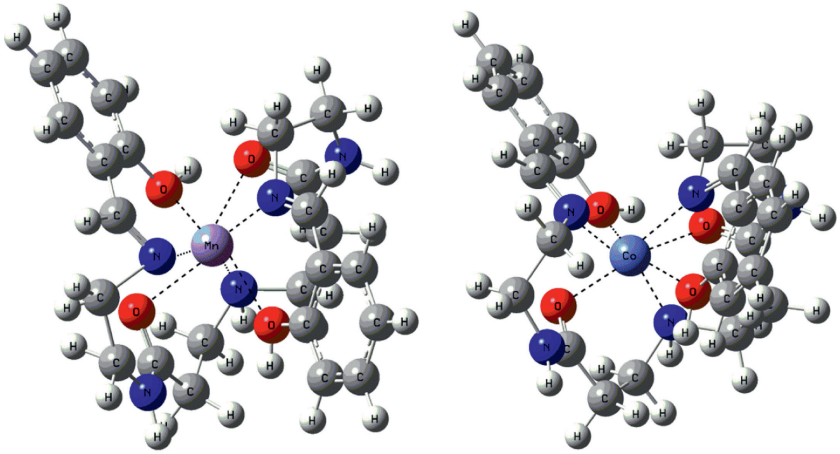

Fig. 4. The optimized geometry of G1.0-SA-Mn(II) and G1.0-SA-Co(II) complexes(B3LYP/6-31 + G(d) for C, H, N, O, and LAN2DZ for Mn(II) and Co(II)).

The adsorption mechanism of the adsorbents for Mn(II) and Co(II) was demonstrated by density functional theory (DFT) calculation. The branching unit of SiO_2-G1.0-SA was chosen as computing model (SiO_2-G1.0-SA) due to the high geometric asymmetry of dendrimer structure. The optimized geometry of the complexes that formed by G1.0-SA with Mn(II) or Co(II) are illustrated in Fig. 4 and the corresponding bond lengths are presented in Table S6 (Supporting information). G1.0-SA chelates with Mn(II) or Co(II) with two hydroxyl O atoms (O1 and O2), two carbonyl O atoms (O3 and O4), one tertiary amine N atom (N1), and two imino N atoms (N2 and N3) to heptacoordinated complexes. The bond lengths that formed by Mn(II) and carbonyl O atoms are 2.33 and 3.24 Å, while that of Mn(II) with hydroxyl O atoms are 1.85 and 2.35 Å. The result suggests that the interaction between hydroxyl O atoms and Mn(II) is higher than that of carbonyl O atoms. The bond lengths of Mn-N formed by imino N atoms are 1.97 and 2.08 Å, whereas that of Mn-N with tertiary amine N atom is 2.41 Å. The difference of the Mn-N bond lengths indicates the binding affinity of imino N atoms is superior than that of tertiary amine N atom. For G1.0-SA-Co(II) complex, the Co-O bond lengths that formed by carbonyl O atoms are 2.03 and 3.44 Å, and that of Co-O with hydroxyl O atoms are 2.03 and 2.47 Å. The bond lengths of Co-N are 2.12 and 2.98 Å, as well as 2.17 Å for imino N and tertiary amine N atoms, respectively.

On the basis of geometry optimization, the interaction mechanism between G1.0-SA with Mn(II) and Co(II) was demonstrated by natural bond orbital (NBO) analysis. The NBO partial charges of Mn(II) and Co(II) in the complexes of G1.0-SA-Mn(II) and G1.0-SA-Co(II) are 1.11 and 1.16, which are lower than the charge of bare Mn(II) and Co(II). The fact suggests the existence of charge transfer from G1.0-SA to metal ion during the adsorption. Second-order perturbation theory analysis is an efficient tool to evaluate the interaction between functional group and metal ion. The stabilization energy ($E(2)$) obtained from second-order perturbation theory analysis can be used to determine the strength of the interaction [20]. Take G1.0-SA-Mn(II) complex for example, the $E(2)$ values are presented in Table S7 (Supporting information). The $E(2)$ values of charge transfer from hydroxyl O atoms to Mn(II) are 9.59 and 11.90 kcal/mol, while that of charge transfer from carbonyl O atoms to Mn(II) are 1.86 and 4.71 kcal/mol. The comparison of the $E(2)$ values further suggests that the interaction between hydroxyl O atoms and Mn(II) is stronger than that of carbonyl O atoms. For N atoms, the $E(2)$ values of charge transfer from imino N atoms to Mn(II) are 13.58 and 27.05 kcal/mol, whereas that of charge transfer from tertiary amine N atom to Mn(II) is 11.10 kcal/mol. The difference between the $E(2)$ value of imino N and tertiary amine N atom demonstrates the binding ability of imino N atoms is superior to that of tertiary amine N atom for Mn(II). Furthermore, the $E(2)$ values of charge transfer from N atoms to Mn(II) are higher than that of O atoms to Mn(II), suggesting imino N and tertiary amine N atoms are the main contributor during the adsorption.

The reproducibility of the adsorbents was determined by using 5% thiourea-0.5 mol/L HNO_3 solution as eluent and the result is shown in Fig. S4 (Supporting information). It can be seen that the adsorbents can be efficiently regenerated by the selected eluent. The regeneration rates of SiO_2-G0-SA, SiO_2-G1.0-SA and SiO_2-G2.0-SA after adsorption of Mn(II) are 98.65%, 97.34%, and 98.32%, while for Co(II) are 97.89%, 96.52%, and 97.20%, respectively. The result indicates that the adsorbents can be reused with practical value.

In summary, Schiff base functionalized PAMAM dendrimer/silica were synthesized and used for the removal of Mn(II) and Co(II). The optimum adsorption pH for Mn(II) and Co(II) are 4 and 6. Adsorption kinetic indicates the adsorption equilibrium time for both metal ions is 120 min. The as-prepared adsorbents exhibit competitive adsorption performance and the maximum adsorption capacity for Mn(II) and Co(II) are 0.92 and 0.94 mmol/g. The adsorbents can be efficiently regenerated using 5% thiourea-0.5 mol/L HNO_3 solution as eluent. The excellent adsorption performance enables them to be efficient adsorbents for the potentially decontamination of aqueous Mn(II) and Co(II).

Declaration of competing interest

The authors declare that they have no known competing financial interests or personal relationships that could have appeared to influence the work reported in this paper.

Acknowledgments

This work was supported by the National Natural Science Foundation of China (No. 21307053), Natural Science Foundation of Shandong Province (No. ZR2018MB039), Science and Technology Research Program of Yantai (No. 2017ZH060).

Appendix A. Supplementary data

Supplementary material related to this article can be found, in the online version, at doi:https://doi.org/10.1016/j.cclet.2020.04.036.

References

[1] D.H. Dai, Z. Li, J. Yang, et al., J. Am. Chem. Soc. 141 (2019) 4756–4763.
[2] M. Huang, Y. Zhang, W. Xiang, et al., J. Environ. Sci. China 85 (2019) 56–65.
[3] L.P. Lingamdinne, J.R. Koduru, H. Roh, et al., Hydrometallurgy 165 (2016) 90–96.
[4] W. Tang, J. Gong, L. Wu, et al., Chemosphere 165 (2016) 277–283.
[5] C. Ling, Y.X. Zhao, Z.X. Ren, et al., Chin. Chem. Lett. 30 (2019) 2196–2200.
[6] X.C. Li, T.R. Lu, Y. Wang, Y.F. Yang, Chin. Chem. Lett. 30 (2019) 2318–2322.
[7] M.E.A. Ali, M.M.S. Aboelfadl, A.M. Selim, H.F. Khalil, G.M. Elkady, Sep. Sci. Technol. 53 (2018) 2870–2881.
[8] Z. Zhang, Y. Niu, H. Chen, et al., ACS Sustain. Chem. Eng. 7 (2019) 7324–7337.
[9] G. Yuan, H. Tu, M. Li, et al., Appl. Surf. Sci. 466 (2019) 903–910.
[10] G. Li, H. Hao, Y. Zhuang, Z. Wang, B. Shi, Water Res. 156 (2019) 287–296.
[11] M. Sajid, M.K. Nazal, Ihsanullah, et al., Sep. Purif. Technol. 191 (2018) 400–423.
[12] X. Song, Y. Niu, Z. Qiu, et al., Fuel 206 (2017) 80–88.
[13] S. Radi, C. El Abiad, N.M.M. Moura, M.A.F. Faustino, M. Neves, J. Hazard. Mater. 370 (2019) 80–90.
[14] X.H. Zhu, W. Jiang, W.R. Cui, et al., Chin. Chem. Lett. 30 (2019) 1133–1136.
[15] X.Z. Wu, P. Liu, Q.S. Pu, et al., Talanta 62 (2004) 918–923.
[16] Y.J. Jiang, Q.M. Gao, H.G. Yu, Y.R. Chen, F. Deng, Microporous Mesoporous Mater. 103 (2007) 316–324.
[17] Y. Niu, R. Qu, C. Sun, et al., J. Hazard. Mater. 244-245 (2013) 276–286.
[18] Y. Niu, R. Qu, H. Chen, et al., J. Hazard. Mater. 278 (2014) 267–278.
[19] X. Song, Y. Niu, P. Zhang, et al., Fuel 199 (2017) 91–101.
[20] D. Schweinfurth, M.G. Sommer, M. Atanasov, et al., J. Am. Chem. Soc. 137 (2015) 1993–2005.
[21] I. Kara, D. Tunc, F. Sayin, S.T. Akar, Appl. Clay Sci. 161 (2018) 184–193.
[22] N. Rajic, D. Stojakovic, S. Jevtic, et al., J. Hazard. Mater. 172 (2009) 1450–1457.
[23] M.D. Meitei, M.N.V. Prasad, Ecol. Eng. 71 (2014) 308–317.
[24] Y.S. Ho, Water Res. 40 (2006) 119–125.
[25] Y. Liu, J. Bai, H. Duan, X. Yin, Chin. J. Chem. Eng. 25 (2017) 32–36.
[26] A.A. Bakr, N.A. Sayed, T.M. Salama, et al., Chem. Intermediat. 44 (2018) 389–405.
[27] D.S.P. Franco, J.M. Cunha, G.F. Dortzbacher, G.L. Dotto, Process Safe. Environ. 109 (2017) 55–62.
[28] G.E. Boyd, A.W. Adamson, L.S. Myers, J. Am. Chem. Soc. 69 (1947) 2836–2848.
[29] D. Reichenberg, J. Am. Chem. Soc. 75 (1953) 589–597.
[30] H.T. Fan, W. Sun, B. Jiang, et al., Chem. Eng. J. 286 (2016) 128–138.
[31] Y.A. Aydin, N.D. Aksoy, Chem. Eng. J. 151 (2009) 188–194.
[32] Q.S. Huang, W. Wu, W. Wei, et al., Chem. Eng. J. 381 (2020) 122632.
[33] T. Fu, Y. Niu, Y. Zhou, et al., J. Taiwan Inst. Chem. E. 97 (2019) 189–199.